

# Imine-Linked Covalent Organic Frameworks: A Biocompatible and pH-Dependent Carrier for In Vitro Sustained Release of Doxorubicin

Nazanin Mokhtari, Mohammad Dinari,\* and Fatemeh Khosravi Esmaeiltarkhani

Cite This: *ACS Omega* 2023, 8, 25565–25573

Read Online

ACCESS |



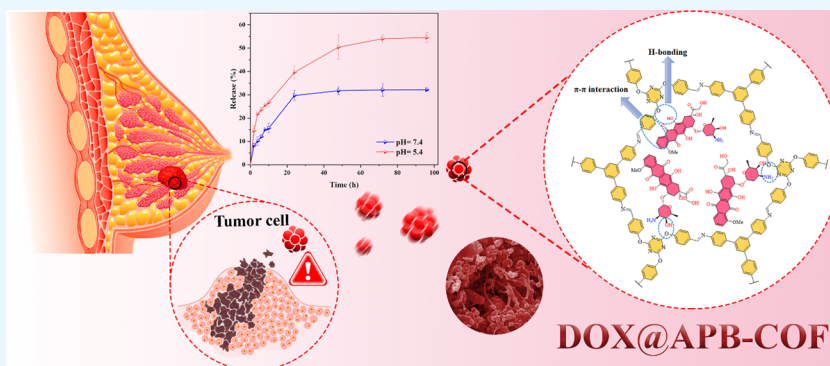
Metrics &amp; More



Article Recommendations



Supporting Information



**ABSTRACT:** Among the novel drug delivery systems (DDSs), covalent organic frameworks (COFs) show promising features in pharmaceutical science. In this paper, an imine-linked COF with hexagonal topology was synthesized using the autoclave condition. Then, the prepared COF (APB-COF) was used as a pH-dependent carrier for in vitro release of doxorubicin (DOX). The intrinsic properties of APB-COF caused reaching an excellent drug encapsulation efficiency. DOX@APB-COF shows an exemplary pH-dependent release in two different pHs. DOX release at pH = 7.4 was 32%, which increased to 54% by changing the pH to the cancer cell pH (pH = 5.4). Moreover, the cytotoxicity of APB-COF and DOX@APB-COF was studied using the standard MTT test against MCF10 (normal breast cell line) and MDAMB231 cells (breast cancer cell line), respectively. It was observed that the APB-COF does not affect cell proliferation, whereas the DOX@APB-COF only limits cancer cell proliferation. Using APB-COF as the drug carrier can pave the way for using COFs in innovative DDSs.

## 1. INTRODUCTION

Cancer has become one of the most important leading causes of death in the last decade, and the situation has deteriorated in recent years.<sup>1</sup> Breast cancer has specific importance among all types of cancer due to its prevalence.<sup>2</sup> Several therapeutic methods have been developed to overcome this significant issue, including photodynamic therapy, radiotherapy, surgery, and chemotherapy.<sup>3</sup> Meanwhile, chemotherapy overtook surgery's importance and became the most widely used method for treating tumors.<sup>4</sup> In chemotherapy, the anticancer drugs irrelevant to the adopting route (body cavity administration, intravenous or even oral, etc.) will spread throughout the body and affect all organs and tissues, whether sick or healthy, targeted or non-targeted, which causes in most cases secondary and adverse side effects.<sup>5</sup> Doxorubicin (DOX) is one of those chemotherapy drugs with intense activity toward breast cancer treatment. Various side effects have been reported for DOX, including nausea and vomiting, hair loss, gastrointestinal disturbances, anemia, thrombocytopenia, hyperpigmentation of the nails, and hypersensitivity (fever, chills, and urticaria).<sup>6</sup> Thus, drug delivery systems (DDSs) with nano-sized carriers were developed to solve this significant issue. DDSs have lower

side effects, targeted drug delivery, and high drug-loading capacity, making them excellent alternatives for traditionally used anticancer drugs. Another significant issue that should be considered is the low drug encapsulation efficiency (DEE) of DOX in drug carriers. Traditionally, triethylamine was used to convert hydrophilic DOX-hydrochloride to the hydrophobic one by removing HCl. However, this method can change the drug activity.<sup>7</sup> In this regard, various nano-sized materials have been reported and systematically investigated for being used as carriers in DDSs. Mesoporous silica, liposomes, layered double hydroxides (LDHs), and metal–organic frameworks (MOFs) are among the most widely used carriers reported in the literature.<sup>8</sup> However, LDHs and MOFs suffer from low chemical stability in acidic medium. Also, they often contain heavy

Received: May 12, 2023

Accepted: June 21, 2023

Published: July 3, 2023



elements in their structure that can cause further toxicity. Therefore, seeking novel porous organic materials with responsive-release features and excellent drug-loading capacity is still the subject of research by many groups worldwide.

Among the new generations of porous materials, using covalent organic frameworks (COFs) in DDSs has gained significant attention in recent years.<sup>9</sup> In contrast to traditional polymeric materials, COFs were prepared from reversible bond-forming reactions rendering crystallinity and biodegradability in such materials.<sup>10</sup> Their porous structure can be modified for pore size, shape, and functional groups.<sup>11</sup> This regularity in their scaffold can simplify the drug release behavior compared to amorphous analogues.<sup>12</sup> Their undeniable excellent properties like high thermal<sup>13</sup> and chemical stability,<sup>14</sup> high specific surface area,<sup>15</sup> low density, tunable structures, and predictable pore size<sup>16</sup> made them be used in various branches of science, including biomedical sciences,<sup>17</sup> optoelectronics,<sup>18</sup> gas separation and storage,<sup>19</sup> catalysis,<sup>20</sup> sensing,<sup>21</sup> and water treatment.<sup>22</sup> For instance, PI-2-COF and PI-3-COF were synthesized in 2016<sup>23</sup> and were used to investigate the load and release of captopril, ibuprofen, and 5-fluorouracil. Rather than the excellent loading and sustained release, these two COFs have outstanding biocompatibility regarding the cell viability test. In another study, DOX encapsulated an imine-based COF in an *in situ* process.<sup>24</sup> The prepared formulation in this study successfully passed the *in vitro* and *in vivo* tests. However, it suffers from a fast release that is not satisfactory for DDSs. It is important to note that the imine-based COFs containing large quantities of imine functionalities can interact with hydrochloride groups to increase drugs' hydrophobicity and a subsequent increase in the loading parameters.

Considering the characteristics of COFs, an imine-linked COF (APB-COF) was prepared through an acid-catalyzed solvothermal condensation reaction, characterized, and used as a vehicle for DOX delivery. The physicochemical features of DOX-loaded COF (DOX@APB-COF) were investigated in the case of drug release kinetics, morphology, drug loading, and encapsulation efficiency. The cytocompatibility of APB-COF against normal breast cells (MCF10 cell line) was evaluated. Also, to consider the antitumor activity of the prepared DOX@APB-COF, the cell viability test against the breast cancer cell line (Mda-mb231 cells) was investigated.

## 2. MATERIALS AND METHODS

**2.1. Materials.** All the materials used in this paper, including 1,2-dichlorobenzene, acetone, dichloromethane, tetrabutylammonium bromide (TBAB), sodium hydroxide, hydrazine hydrate, ethanol, 2,4,6-trichloro-1,3,5-triazine (TCT), tetrahydrofuran (THF), *p*-hydroxybenzaldehyde, *N,N*-dimethylformamide (DMF), methanol, 4-nitroacetophenone, toluene, trifluoromethanesulfonic acid, mesitylene, dioxane, acetic acid, ethyl acetate, and hydrochloric acid, were analytically pure, obtained from Merck and Aldrich Chemical companies, and used without further purification.

**2.2. Synthesis of 2,4,6-Tris(4-formyl phenoxy)-1,3,5-triazine (TFPT).** TFPT was synthesized using a procedure reported elsewhere.<sup>25</sup> *p*-Hydroxybenzaldehyde (4.88 g) was dissolved in 50 mL of deionized (DI) water with the help of 1.60 g of sodium hydroxide. Then, a solution of 1.84 g of TCT and 0.02 g of TBAB in 50 mL of dichloromethane was added to form a biphasic solution. The mixture was stirred for 24 h at room temperature. Afterward, the organic phase was separated and washed with 3 × 25 mL of NaOH solution (10% wt/wt) and 2 ×

20 mL of DI water. Finally, the obtained powder from the evaporation of the organic phase was recrystallized from ethyl acetate.

**2.3. Synthesis of 1,3,5-Tris(4-nitrophenyl)benzene (TNPB).** TNPB was synthesized in a condensation reaction reported in the literature.<sup>26</sup> 4-Nitroacetophenone (5 g) and CF<sub>3</sub>SO<sub>3</sub>H (0.2 mL) were added to 20 mL of dried toluene. Then, the mixture was equipped with a Dean–Stark water separator and let to reflux for 48 h. The completion of the reaction was confirmed by the amount of water separated in the azeotropic distillation. The mixture was cooled to room temperature and filtered. Finally, the obtained solid was washed with refluxing DMF to yield a pale-yellow solid that is not soluble in common solvents.

**2.4. Synthesis of 1,3,5-Tris(4-aminophenyl)benzene (TAPB).** The prepared TNPB (2 g) from the previous step and 0.4 g of Pd/C (10 wt %) were dispersed in 40 mL of ethanol. Then, 6 mL of hydrazine hydrate (80 wt %) was added dropwise, and the prepared mixture was refluxed under the N<sub>2</sub> atmosphere for 12 h. Finally, the mixture was hot-filtered, and the filtrate was concentrated to yield the product.

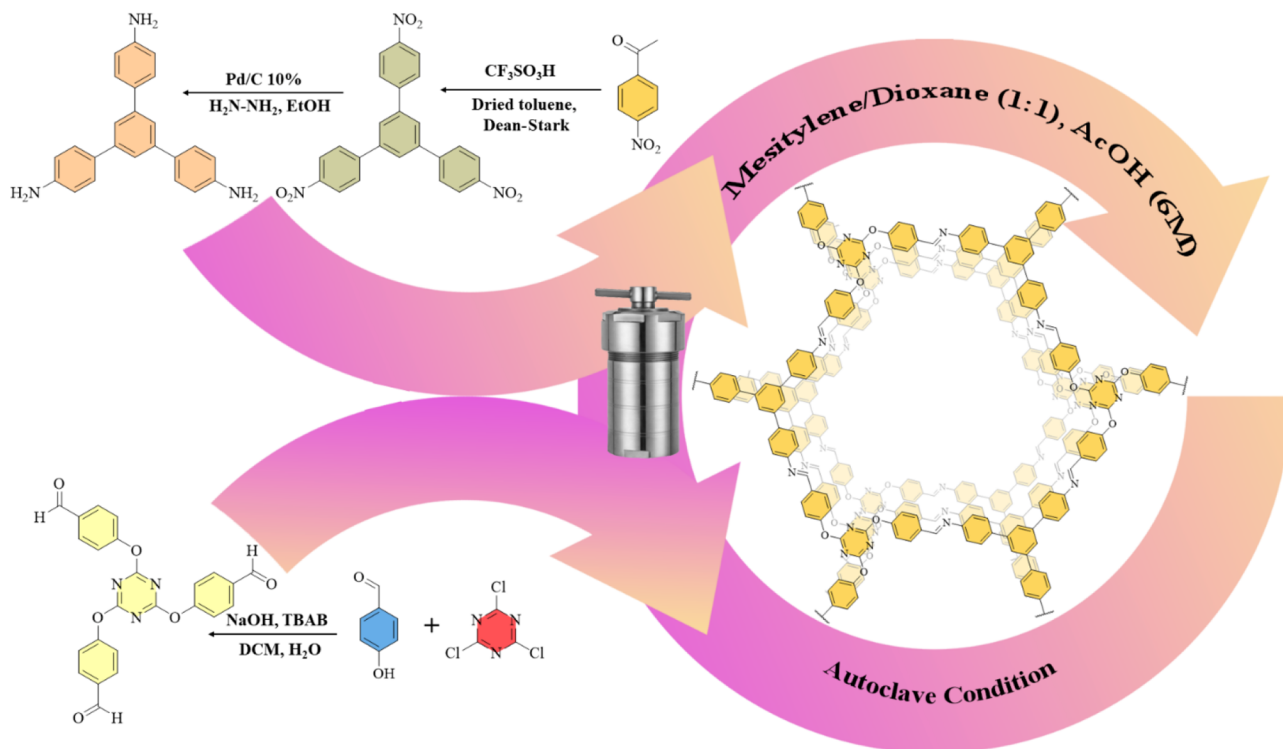
**2.5. Synthesis of APB-COF.** An autoclave reactor was utilized for the synthesis of APB-COF. Briefly, 0.089 g (0.2 mmol) of TFPT and 0.079 g (0.2 mmol) of TAPB were added to 7 mL of mesitylene/dioxane (1:1 v/v) solution. The obtained homogeneous mixture, upon exposure to ultrasound irradiation, was charged with 0.75 mL of acetic acid (6 mol L<sup>-1</sup>), and the reactor was heated to 120 °C for 5 days. Finally, the yellow fluffy powder was separated by centrifugation and washed with a large amount of THF, acetone, and chloroform.

**2.6. Preparation of DOX@APB-COF.** The APB-COF:DOX ratio was optimized in a typical procedure based on the contact time. In this regard, a specific amount of APB-COF was immersed in 5 mL of PBS solution (pH = 7.4) containing different amounts of DOX in a way that the carrier:drug ratio was fixed to 1:10, 1:20, and 1:40 (wt/wt). The mixture was sonicated for 1 h, stirred for 6, 12, and 24 h, and then centrifuged. Considering the initial DOX concentration and the concentration in the supernatant solution using a UV–vis spectrophotometer, the DEE can be calculated by the following equation:<sup>27</sup>

$$\text{DEE (\%)} = \left( \frac{\text{the total amount of DOX added} - \text{free DOX}}{\text{the total amount of DOX added}} \right) \times 100 \quad (1)$$

**2.7. In Vitro Drug Release Study.** The DOX release was studied by placing 1 mL of suspension of DOX@APB-COF with a concentration of 2 mg mL<sup>-1</sup> in dialysis bags in pH = 5.4 and pH = 7.4, which are the endosomal pH of cancer cells and the physiological pH, respectively. The bags were soaked in 24 mL of the corresponding buffer solutions at 37 °C. In each time interval, 2 mL of the medium was taken, and the amount of DOX in the solution was evaluated using the UV–vis spectrometer at 490 nm. Then, the cumulative drug release (CDR) was calculated using the following equation:<sup>3</sup>

## Scheme 1. Schematic Illustration of APB-COF



$$\text{CDR (\%)} = \left( \frac{\text{weight of released DOX in PBS buffer solution}}{\text{weight of DOX in nanotubes}} \right) \times 100 \quad (2)$$

The release mechanism was studied by fitting the release data into five kinetic models, i.e., Higuchi, zero-order, first-order, Baker–Lonsdale, and Korsmeyer–Peppas. Among all these equations, the Korsmeyer–Peppas model can predict the Fickian or non-Fickian mechanism of release. The equations and detailed information are discussed in the [Supporting Information](#).

**2.8. Cell Viability Assay.** MCF10 and Mda-mb231 cell lines, as normal and breast cancer cells, respectively, were cultured in a medium containing 1% antibiotic (penicillin/streptomycin), 10% FBS, in 5% CO<sub>2</sub>, and 95% humidity at 37 °C in an incubator. After 24 h of incubation, the cells were collected and transferred into a 96-well plate. Then, the cells were treated with various concentrations of APB-COF and DOX@APB-COF (25, 50, 75, 100, 250, 500, 750, 1000, and 2500 mg L<sup>-1</sup>). The incubation continued for 72 h, MTT solution was added, and the cell viability was determined using an ELISA plate reader at 570 nm after 2 h.

### 3. RESULTS AND DISCUSSION

Preparing APB-COF was initiated by synthesizing two building blocks with C<sub>3</sub> symmetries. Through the condensation reaction between the TFPT and TAPB, a 2D framework was prepared with the hexagonal topology. [Scheme 1](#) summarizes the synthesis procedure of APB-COF in which the building blocks reacted in an autoclave using mesitylene/dioxane/acetic acid (6 mol L<sup>-1</sup>) with a ratio of 1/1/0.75 at 120 °C for 5 days. Using an

autoclave can demonstrate a new approach toward the large-scale synthesis of COFs.

**3.1. Characterization of APB-COF.** Fourier transform infrared (FTIR) spectroscopy of APB-COF and its building blocks are depicted in [Figure 1](#). The triazine –C=N–

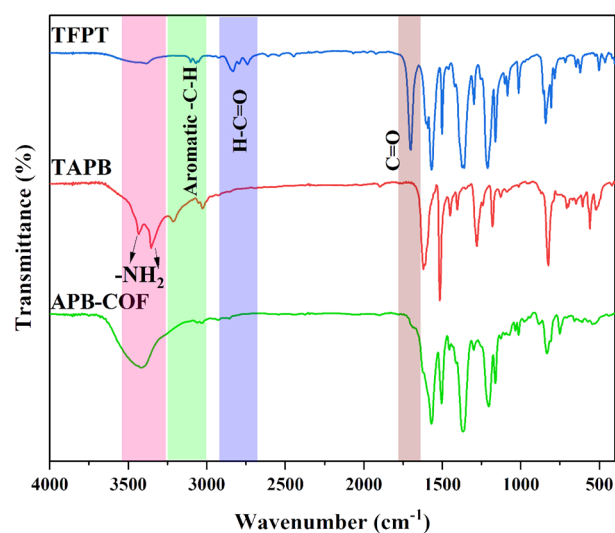


**Figure 1.** FTIR spectra of TFPT, TAPB, and APB-COF.

characteristic peaks were observed at 1560 cm<sup>-1</sup>. The aldehydic C–H of the characteristic band at 2875 and 2779 cm<sup>-1</sup> and the carbonyl stretching band at 1699 cm<sup>-1</sup> disappeared upon the condensation reaction with amine groups in TAPB. Similarly, the N–H stretching mode at 3435 and 3350 cm<sup>-1</sup> and bending mode at 1430 cm<sup>-1</sup> were also omitted in APB-COF due to the efficient condensation reaction. Also, the FTIR spectra of 4-nitroacetophenone, TNPB, and TAPB are depicted in [Figure S1](#).

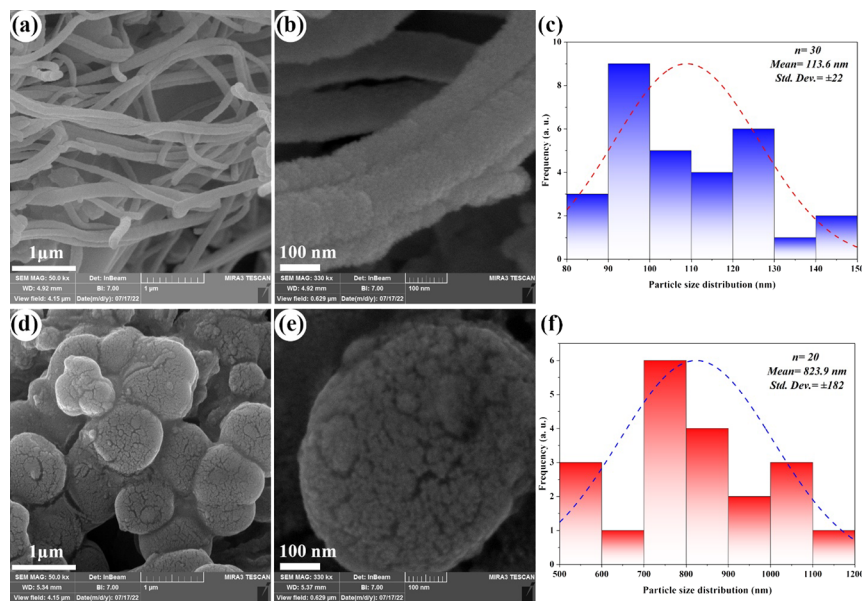


**Figure 2.** (a, b) FESEM images of APB-COF, (c) its corresponding particle size distribution diagram, (d, e) FESEM images of DOX@APB-COF, and (f) its corresponding particle size distribution diagram.

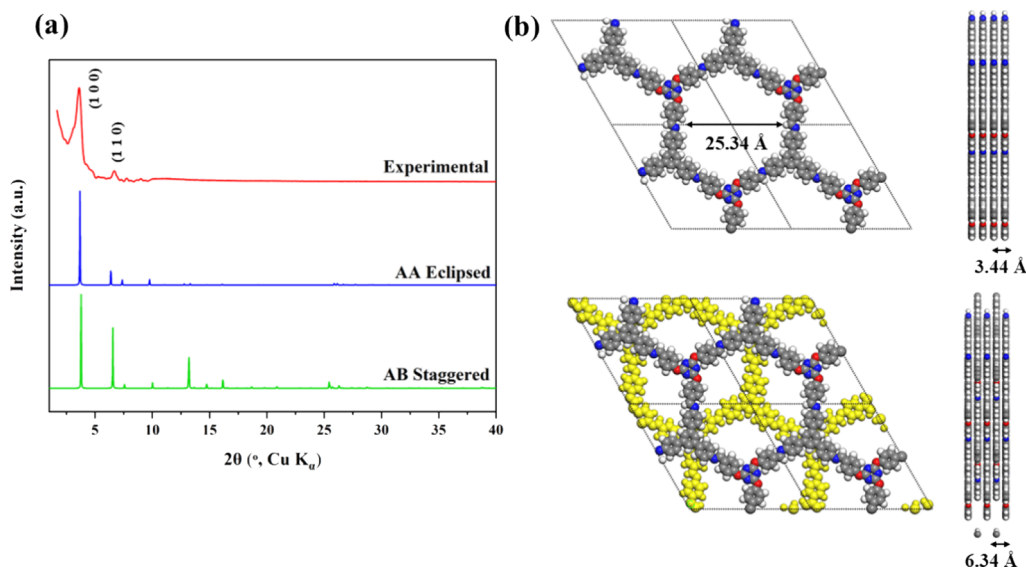


**Figure 3.** (a) Experimental and simulated eclipsed and staggered PXRD patterns of the APB-COF and (b) corresponding front and side views of the eclipsed and staggered forms of APB-COF.

The  $^1\text{H}$  NMR spectra of TFPT and TAPB are shown in Figures S2 and S3, respectively. Thermogravimetric analysis of the prepared APB-COF shows excellent thermal stability up to 350 °C. The obtained char yield at 800 °C was 23%, while the  $T_{5\%}$  and  $T_{10\%}$  were 147 and 332 °C, respectively (Figure S4). The mass loss at temperatures lower than 100 °C corresponded to the physisorbed solvents, and the mass loss at around 400 °C is attributed to the imine bond decomposition.

The field emission scanning electron microscopy (FESEM) images (Figure 2) of APB-COF show that it was crystallized in uniform nanofibers with a mean diameter of 113 nm, implying excellent porosity in its structure. After the loading of DOX into these nanofibers, the morphology of DOX@APB-COF was changed into spheres, proving the efficient drug loading (Figure 2d,e). Moreover, the mean particle size was increased to 824 nm after loading. Comparing the morphology of APB-COF in this

paper with the FESEM images in the literature reveals slight differences that could be attributed to the preparation method.<sup>28</sup>

The experimental and simulated powder X-ray diffraction (PXRD) pattern of the prepared APB-COF is depicted in Figure 3. Two distinct peaks were observed at 3.60 and 6.69° attributed to the (100) and (110) diffractions, respectively. The obtained data is consistent with previously reported diffraction positions.<sup>28</sup> The universal force field and the Ewald summation of the *Forcite* module in the Materials Studio software package were used to elucidate the constitution of the framework. The unit cell parameters of the AA stacking form of the  $P_6$  hexagonal space group simulated to be  $a = b = 27.68(0831)$  Å,  $c = 3.44(1436)$  Å,  $\alpha = \beta = 90^\circ$ , and  $\gamma = 120^\circ$ , while the AB stacking unit cell parameters were found to be  $a = b = 27.68(1808)$  Å,  $c = 6.34(0911)$  Å,  $\alpha = \beta = 90^\circ$ , and  $\gamma = 120^\circ$ . The obtained experimental PXRD AA stacking form is better described in the

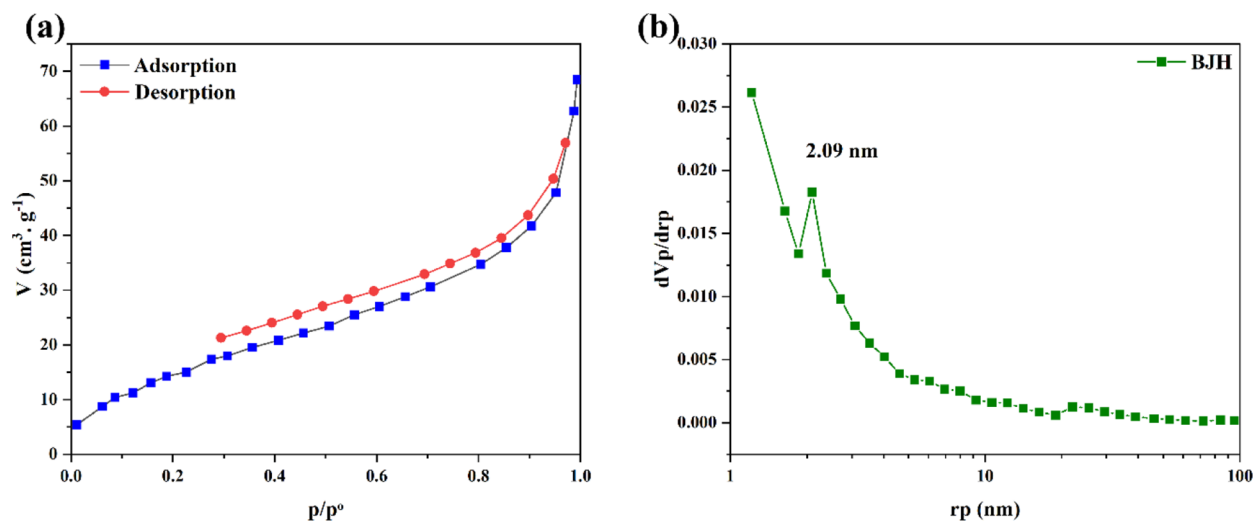


Figure 4. (a)  $N_2$  adsorption/desorption isotherm of APB-COF and (b) pore width distribution diagram.

$P_{-6}$  hexagonal space group. Using the *Forcite* module is more common in predicting the PXRD pattern than DFTB+, which is used in a similar study.<sup>28</sup>

The  $N_2$  sorption/desorption isotherms of APB-COF at 77 K are shown in Figure 4a. The specific surface area is determined to be  $61 \text{ m}^2 \text{ g}^{-1}$ . Also, the pore size distribution diagram (Figure 4b) shows a mean pore diameter of 2.09 nm, consistent with the data obtained from the simulated PXRD. According to the IUPAC classification of the gas adsorption,<sup>29</sup> the obtained isotherm and hysteresis loop agree with types I and H4, respectively.

**3.2. DOX Loading and In Vitro Release from DOX@APB-COF.** The drug loading and its release behavior in DDSs are essential characteristics that should be explored. The preliminary studies reveal that the loading process is directly affected by the pH of the loading medium. In an acidic medium, the loading was unsatisfactory; thus, the drug-to-carrier ratio was optimized (Table 1) at pH = 7.4 to gain the highest DEE (%). In this regard, the DOX:APB-COF ratio was selected to be 1:10 to use a lower carrier usage, while the DEE reaches 94%.

Table 1. Formulations and Influential Factors on the Drug-Loading Process

entry	formulation (DOX:APB-COF)	DEE (%)		
		6 h	12 h	24 h
1	1:10	72	81	94
2	1:20	84	92	98
3	1:40	>99	>99	>99

The physicochemical condition (PBS, 37 °C, pH = 7.4) and the tumor extracellular region (PBS, 37 °C, pH = 5.4) were simulated, and the DOX release was studied to assess the viability of using APB-COF as an anticancer DDS. As evidenced in Figure 5, the DOX release at pH = 7.4 was lower than that of pH = 5.4. After 72 h, the release reached only 32%, while the DOX release at pH = 5.4 reached 54%. This observation seems to be attributed to the interactions between DOX and APB-COF that are not changed significantly under physicochemical conditions. More importantly, the higher release in the acidic medium can be explained by the electrostatic interactions. While the electrostatic interactions were decreased over changing the

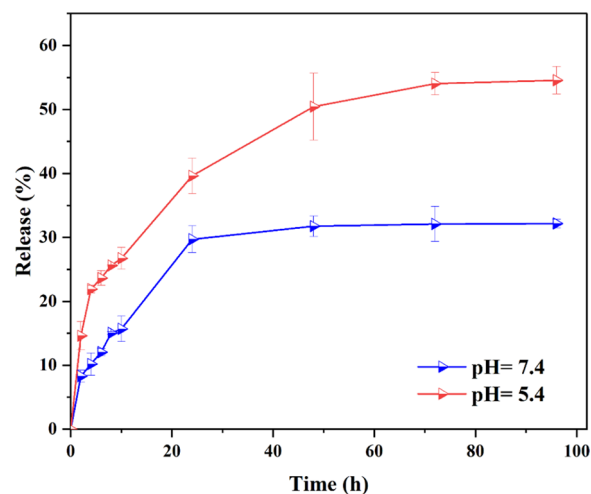
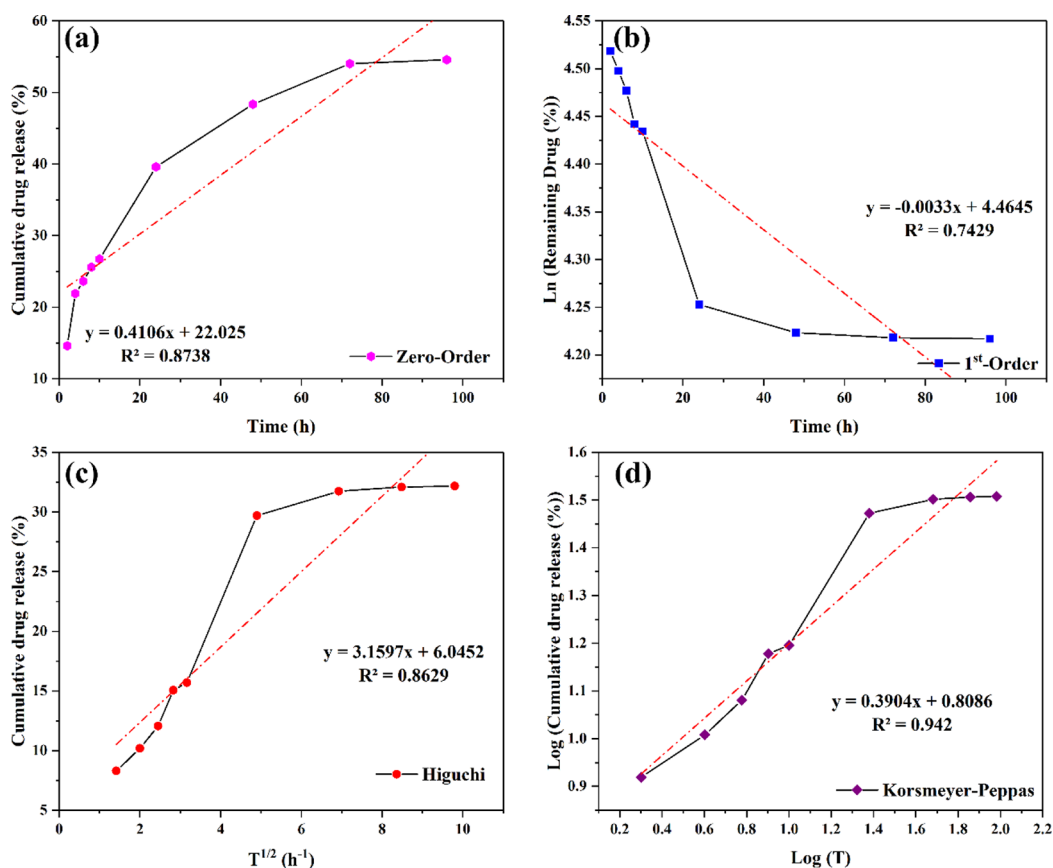


Figure 5. DOX release from APB-COF in simulated physicochemical conditions (PBS, 37 °C, pH = 7.4) and the cancer cell acidic medium (PBS, 37 °C, pH = 5.4).

pH value to 5.4, the electrostatic repulsion was enhanced between the drug and APB-COF due to the possible protonation of imine linkages, triggering the drug release. This pH-dependent release feature presented in DOX@APB-COF can protect normal cells from DOX side effects. Therefore, considerable amounts of incorporated DOX remain in the APB-COF structure by staying in plasma (pH = 7.4). DOX is only released after reaching the carrier to the cancer cells, internalized by endocytosis, and exposed to the acidic medium (pH = 5.4). The faster and enhanced release might occur inside the endosome/lysosome due to the lower pH values increasing DOX@APB-COF efficiency.

**3.3. In Vitro Release Kinetic and Mechanism Investigation.** The obtained release results were fitted to different kinetic models, including Korsmeyer–Peppas, Higuchi, first-order, and zero-order, summarized in Figures 6 and 7 and Table 2. The respective squared correlation coefficient ( $R^2$ ) values were used to determine the best-fitted model for the DOX release from DOX@APB-COF. According to Table 2 and Figures 6 and 7, the DOX release follows the Korsmeyer–Peppas model as the best-fitted model. Rather than the mechanism, this model can represent some information about



**Figure 6.** Fitted kinetic models to the release results at pH = 7.4 for APB-COF: (a) zero-order, (b) first-order, (c) Higuchi, and (d) Korsmeyer–Peppas.

the release mechanism. Accordingly, in eq 3,  $n$  is the release exponent,  $t$  is the time,  $k$  is the release rate constant, and  $M_t/M_\infty$  is the DOX released fraction.<sup>30</sup>

$$\frac{M_t}{M_\infty} = kt^n \quad (3)$$

The value of  $n$  can provide a mechanistic sight to the release mechanism. According to the literature, for  $n \leq 0.45$ , the drug release follows the case I diffusion (Fickian), for  $0.45 < n < 0.89$  follows the anomalous diffusion (non-Fickian), for  $n = 0.89$  follows the zero-order (case II transport) release, and for  $n > 0.89$  follows the super case II transport. The release mechanism could be one of these or a combination of them. The APB-COF carrier shows a release exponent of 0.39 and 0.34 for pH = 5.4 and pH = 7.4, respectively.<sup>31</sup> In this case, the DOX penetration process is derived from the concentration gradient.

**3.4. Cell Viability Test.** The standard 3-(4,5-dimethylthiazol-2-yl)-2,5-diphenyltetrazolium bromide (MTT) cell assays were used to explore the cytotoxicity and biocompatibility of APB-COF, DOX, and DOX@APB-COF. The cytotoxicity of APB-COF in concentrations varied from 25 to 2500  $\mu\text{g mL}^{-1}$  by incubation with MCF10 (normal breast cell line) for 72 h (Figure 8a). As evidenced in Figure 8a, APB-COF does not affect the MCF10 cell proliferation at concentrations lower than 250  $\mu\text{g mL}^{-1}$ . Also, the cytotoxicity of APB-COF and DOX@APB-COF against the MDAMB231 cells (breast cancer cell line) was studied (Figure 8b) by incubation of the prepared concentrations (25 to 2500  $\mu\text{g mL}^{-1}$ ). Interestingly, APB-COF does not affect the proliferation of MDAMB231 cells at concentrations lower than 250  $\mu\text{g mL}^{-1}$ , while DOX@APB-

COF inhibits cell proliferation even at 25  $\mu\text{g mL}^{-1}$ . This phenomenon shows the excellent viability of DOX@APB-COF in treating breast cancer. Since APB-COF and DOX@APB-COF cannot be solved in common solvents in higher concentrations, the decrease in cell viability is attributed to cellular suffocation.

## 4. CONCLUSIONS

To increase DEE, different methods have been introduced, and several DDSs were developed. Among them, COFs gained much attention due to their excellent features and ability to remove HCl from drugs with hydrochloride moieties. In this study, TFPT and TAPB were condensed in autoclave conditions to form an imine-linked COF with hexagonal topology. This method is a facile approach for producing COFs on larger scales and maintaining their unique properties. The prepared COF shows a high DOX encapsulation efficiency, a pH-dependent release behavior, and biocompatibility. Changing the pH from physicochemical conditions (PBS, pH = 7.4) to cancer extracellular acidic conditions (PBS, pH = 5.4) has triggered the DOX release. The MTT assay of APB-COF and DOX@APB-COF against MCF10 (normal breast cell line) and MDAMB231 cells (breast cancer cell line) reveals that APB-COF and DOX@APB-COF do not have any toxicity against normal cells, while the cancer cell proliferation was interrupted by DOX@APB-COF even in a concentration of 25  $\mu\text{g mL}^{-1}$ . This type of work can provide a sight of using innovative materials in DDSs.

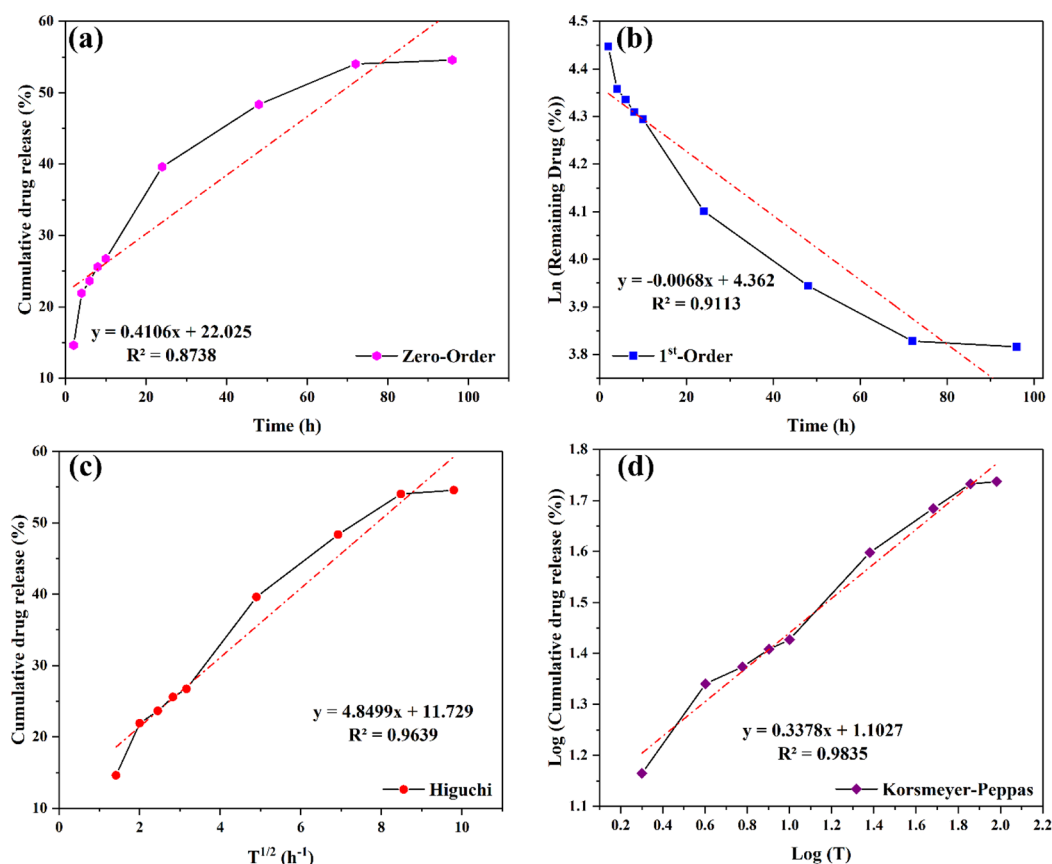


**Figure 7.** Fitted kinetic models to the release results at pH = 5.4 for APB-COF: (a) zero-order, (b) first-order, (c) Higuchi, and (d) Korsmeyer–Peppas.

**Table 2.** Fitted Kinetic Models and Their Corresponding  $R^2$

kinetic models		zero-order	first-order	Higuchi	Korsmeyer–Peppas
squared correlation coefficient ( $R^2$ )	pH = 7.4	0.874	0.743	0.863	0.942
	pH = 5.4	0.874	0.911	0.964	0.984

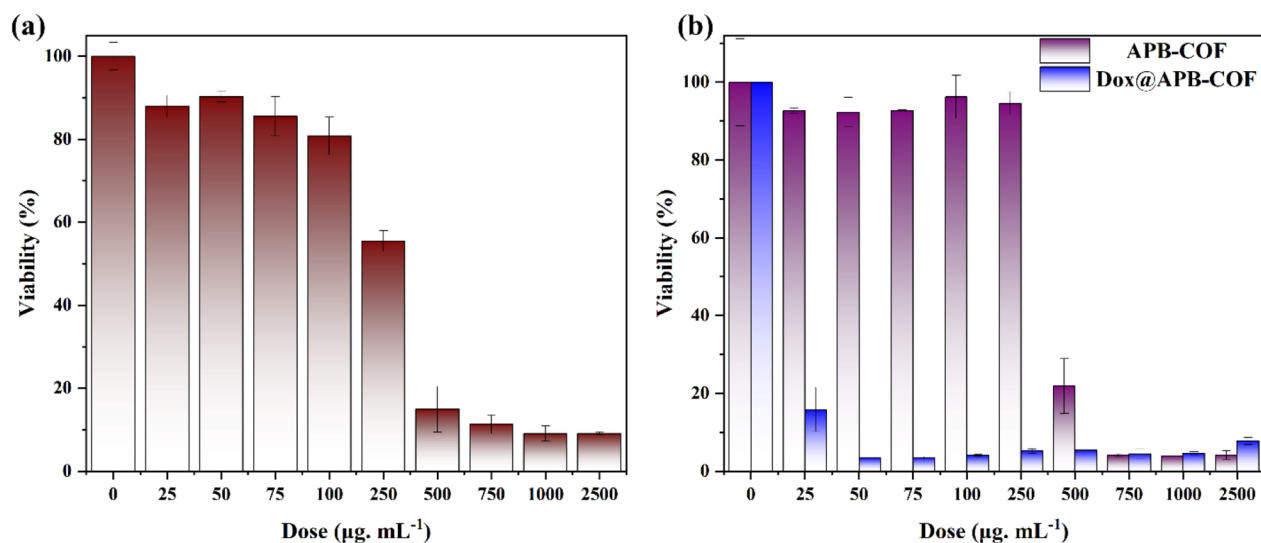


**Figure 8.** (a) Cytotoxicity of APB-COF against MCF10 cells after 72 h of incubation and (b) cytotoxicity of APB-COF and DOX@APB-COF against MDAmb231 cells after 72 h of incubation.

## ■ ASSOCIATED CONTENT

### SI Supporting Information

The Supporting Information is available free of charge at <https://pubs.acs.org/doi/10.1021/acsomega.3c03316>.

Synthesis procedures and <sup>1</sup>H NMR of the building blocks (PDF)

## ■ AUTHOR INFORMATION

### Corresponding Author

Mohammad Dinari – Department of Chemistry, Isfahan University of Technology, Isfahan 84156-83111, Islamic Republic of Iran; [orcid.org/0000-0001-5291-7142](https://orcid.org/0000-0001-5291-7142); Phone: +98-31-3391-3270; Email: [dinari@iut.ac.ir](mailto:dinari@iut.ac.ir), [mdinary@gmail.com](mailto:mdinary@gmail.com); Fax: +98-31-3391-2350

### Authors

Nazanin Mokhtari – Department of Chemistry, Isfahan University of Technology, Isfahan 84156-83111, Islamic Republic of Iran

Fatemeh Khosravi Esmaeilarkhani – Department of Chemistry, Isfahan University of Technology, Isfahan 84156-83111, Islamic Republic of Iran

Complete contact information is available at:

<https://pubs.acs.org/doi/10.1021/acsomega.3c03316>

### Author Contributions

The manuscript was written through contributions of all authors. All authors have given approval to the final version of the manuscript.

### Notes

The authors declare no competing financial interest.

## ■ ACKNOWLEDGMENTS

The authors were thankful to the Research Council of Isfahan University of Technology for their support on this manuscript.

## ■ REFERENCES

- (1) (a) Akhtar, M. J.; Ahamed, M.; Alhadlaq, H. A.; Alrokayan, S. A.; Kumar, S. Targeted anticancer therapy: overexpressed receptors and nanotechnology. *Clin. Chim. Acta* **2014**, *436*, 78–92. (b) Zhang, W.; Li, Y.; Xu, L.; Wang, D.; Long, J.; Zhang, M.; Wang, Y.; Lai, Y.; Liang, X.-J. Near-Infrared-absorbing conjugated polymer nanoparticles loaded with doxorubicin for combinatorial photothermal-chemotherapy of cancer. *ACS Appl. Polym. Mater.* **2020**, *2*, 4180–4187.
- (2) Giaquinto, A. N.; Sung, H.; Miller, K. D.; Kramer, J. L.; Newman, L. A.; Minihan, A.; Jemal, A.; Siegel, R. L. Breast cancer statistics, 2022. *CA: A Cancer Journal for Clinicians* **2022**, *72*, 524–541.
- (3) Mokhtari, N.; Taymouri, S.; Mirian, M.; Dinari, M. Covalent triazine-based polyimine framework as a biocompatible pH-dependent sustained-release nanocarrier for sorafenib: An in vitro approach. *J. Mol. Liq.* **2020**, *297*, No. 111898.
- (4) Liu, S.; Yang, J.; Guo, R.; Deng, L.; Dong, A.; Zhang, J. Facile fabrication of redox-responsive covalent organic framework nanocarriers for efficiently loading and delivering doxorubicin. *Macromol. Rapid Commun.* **2020**, *41*, 1900570.
- (5) Dai, L.; Liu, J.; Luo, Z.; Li, M.; Cai, K. Tumor therapy: targeted drug delivery systems. *J. Mater. Chem. B* **2016**, *4*, 6758–6772.
- (6) Carvalho, C.; Santos, R.; Cardoso, S.; Correia, S.; Oliveira, P.; Santos, M.; Moreira, P. Doxorubicin: the good, the bad and the ugly effect. *Curr. Med. Chem.* **2009**, *16*, 3267–3285.
- (7) (a) Tang, J.; Zhang, R.; Guo, M.; Shao, L.; Liu, Y.; Zhao, Y.; Zhang, S.; Wu, Y.; Chen, C. Nucleosome-inspired nanocarrier obtains encapsulation efficiency enhancement and side effects reduction in chemotherapy by using fullerene assembled with doxorubicin. *Biomaterials* **2018**, *167*, 205–215. (b) Yoo, H. S.; Park, T. G. Folate receptor targeted biodegradable polymeric doxorubicin micelles. *J. Controlled Release* **2004**, *96*, 273–283. (c) Yadav, A. K.; Mishra, P.; Mishra, A. K.; Mishra, P.; Jain, S.; Agrawal, G. P. Development and characterization of hyaluronic acid-anchored PLGA nanoparticulate carriers of doxorubicin. *Nanomed.: Nanotechnol., Biol. Med.* **2007**, *3*, 246–257.
- (8) (a) Manzano, M.; Vallet-Regí, M. Mesoporous silica nanoparticles for drug delivery. *Adv. Funct. Mater.* **2020**, *30*, 1902634. (b) Saraf, S.; Jain, A.; Tiwari, A.; Verma, A.; Panda, P. K.; Jain, S. K. Advances in liposomal drug delivery to cancer: An overview. *J. Drug Delivery Sci. Technol.* **2020**, *56*, No. 101549. (c) Shirin, V. A.; Sankar, R.; Johnson, A. P.; Gangadharappa, H.; Pramod, K. Advanced drug delivery applications of layered double hydroxide. *J. Controlled Release* **2021**, *330*, 398–426. (d) Sun, Y.; Zheng, L.; Yang, Y.; Qian, X.; Fu, T.; Li, X.; Yang, Z.; Yan, H.; Cui, C.; Tan, W. Metal-organic framework nanocarriers for drug delivery in biomedical applications. *Nano-Micro Lett.* **2020**, *12*, 103.
- (9) (a) Wu, M.-X.; Yang, Y.-W. Applications of covalent organic frameworks (COFs): From gas storage and separation to drug delivery. *Chin. Chem. Lett.* **2017**, *28*, 1135–1143. (b) Zhao, Z.; Feng, H.; Qin, D.; Li, W.; Wang, W.; Chen, S. pH-Responsive Intelligent Antibacterial Coatings Based on 2D-COF for Controlled Release of Capsaicin. *ACS Appl. Polym. Mater.* **2023**, *5*, 2124–2135.
- (10) Evans, A. M.; Parent, L. R.; Flanders, N. C.; Bisbey, R. P.; Vitaku, E.; Kirschner, M. S.; Schaller, R. D.; Chen, L. X.; Gianneschi, N. C.; Dichtel, W. R. Seeded growth of single-crystal two-dimensional covalent organic frameworks. *Science* **2018**, *361*, 52–57.
- (11) Zhang, G.; Tsujimoto, M.; Packwood, D.; Duong, N. T.; Nishiyama, Y.; Kadota, K.; Kitagawa, S.; Horike, S. Construction of a hierarchical architecture of covalent organic frameworks via a postsynthetic approach. *J. Am. Chem. Soc.* **2018**, *140*, 2602–2609.
- (12) Sant, S.; Nadeau, V.; Hildgen, P. Effect of porosity on the release kinetics of propafenone-loaded PEG-g-PLA nanoparticles. *J. Controlled Release* **2005**, *107*, 203–214.
- (13) Kim, S.; Choi, H. C. Recent advances in covalent organic frameworks for molecule-based two-dimensional materials. *ACS Omega* **2020**, *5*, 948–958.
- (14) Zhang, J.; Han, X.; Wu, X.; Liu, Y.; Cui, Y. Multivariate chiral covalent organic frameworks with controlled crystallinity and stability for asymmetric catalysis. *J. Am. Chem. Soc.* **2017**, *139*, 8277–8285.
- (15) Xu, H.; Tao, S.; Jiang, D. Proton conduction in crystalline and porous covalent organic frameworks. *Nat. Mater.* **2016**, *15*, 722–726.
- (16) Zhao, W.; Xia, L.; Liu, X. Covalent organic frameworks (COFs): perspectives of industrialization. *CrystEngComm* **2018**, *20*, 1613–1634.
- (17) (a) Bhunia, S.; Deo, K. A.; Gaharwar, A. K. 2D covalent organic frameworks for biomedical applications. *Adv. Funct. Mater.* **2022**, *30*, 2002046. (b) Yazdani, H.; Shahbazi, M.-A.; Varma, R. S. 2D and 3D covalent organic frameworks: Cutting-edge applications in biomedical sciences. *ACS Appl. Bio Mater.* **2022**, *5*, 40–58.
- (18) (a) Keller, N.; Bein, T. Optoelectronic processes in covalent organic frameworks. *Chem. Soc. Rev.* **2021**, *50*, 1813–1845. (b) Mandal, A. K.; Mahmood, J.; Baek, J. B. Two-dimensional covalent organic frameworks for optoelectronics and energy storage. *ChemNanoMat* **2017**, *3*, 373–391.
- (19) (a) Wang, P.; Peng, Y.; Zhu, C.; Yao, R.; Song, H.; Kun, L.; Yang, W. Single-Phase Covalent Organic Framework Staggered Stacking Nanosheet Membrane for CO<sub>2</sub>-Selective Separation. *Angew. Chem., Int. Ed.* **2021**, *60*, 19047–19052. (b) Li, Z.; Zhi, Y.; Feng, X.; Ding, X.; Zou, Y.; Liu, X.; Mu, Y. An azine-linked covalent organic framework: synthesis, characterization and efficient gas storage. *Chem. - Eur. J.* **2015**, *60*, 12079–19052.
- (20) (a) Li, F.; Kan, J. L.; Yao, B. J.; Dong, Y. B. Synthesis of chiral covalent organic frameworks via asymmetric organocatalysis for heterogeneous asymmetric catalysis. *Angew. Chem., Int. Ed.* **2022**, *61*, No. e202115044. (b) Guo, J.; Jiang, D. Covalent organic frameworks for heterogeneous catalysis: principle, current status, and challenges. *ACS Cent. Sci.* **2020**, *6*, 869–879. (c) Liu, J.; Wang, N.; Ma, L. Recent

advances in covalent organic frameworks for catalysis. *Chem. - Asian J.* **2020**, *61*, 338–351.

(21) Afshari, M.; Dinari, M.; Farrokhpour, H.; Zamora, F. Imine-linked covalent organic framework with a naphthalene moiety as a sensitive phosphate ion sensing. *ACS Appl. Mater. Interfaces* **2022**, *14*, 22398–22406.

(22) (a) Mokhtari, N.; Dinari, M.; Fashandi, H. Developing polysulfone-based mixed matrix membrane containing hydrazone-linked covalent organic frameworks towards dye wastewater purification. *Chem. Eng. J.* **2022**, *446*, No. 137456. (b) Xia, Z.; Zhao, Y.; Darling, S. B. Covalent organic frameworks for water treatment. *Adv. Mater. Interfaces* **2021**, *8*, 2001507.

(23) Bai, L.; Phua, S. Z. F.; Lim, W. Q.; Jana, A.; Luo, Z.; Tham, H. P.; Zhao, L.; Gao, Q.; Zhao, Y. Nanoscale covalent organic frameworks as smart carriers for drug delivery. *Chem. Commun.* **2016**, *52*, 4128–4131.

(24) Liu, S.; Hu, C.; Liu, Y.; Zhao, X.; Pang, M.; Lin, J. One-pot synthesis of DOX@ covalent organic framework with enhanced chemotherapeutic efficacy. *Chem. - Eur. J.* **2019**, *25*, 4315–4319.

(25) Mokhtari, N.; Afshari, M.; Dinari, M. Synthesis and characterization of a novel fluorene-based covalent triazine framework as a chemical adsorbent for highly efficient dye removal. *Polymer* **2020**, *195*, No. 122430.

(26) Sun, Q.; Aguila, B.; Perman, J.; Earl, L. D.; Abney, C. W.; Cheng, Y.; Wei, H.; Nguyen, N.; Wojtas, L.; Ma, S. Postsynthetically modified covalent organic frameworks for efficient and effective mercury removal. *J. Am. Chem. Soc.* **2017**, *139*, 2786–2793.

(27) Dinari, M.; Mokhtari, N.; Taymouri, S.; Arshadi, M.; Abbaspourrad, A. Covalent polybenzimidazole-based triazine frameworks: a robust carrier for non-steroidal anti-inflammatory drugs. *Mater. Sci. Eng., C* **2020**, *108*, No. 110482.

(28) Li, Y.; Chen, W.; Hao, W.; Li, Y.; Chen, L. Covalent organic frameworks constructed from flexible building blocks with high adsorption capacity for pollutants. *ACS Appl. Nano Mater.* **2018**, *1*, 4756–4761.

(29) Thommes, M.; Kaneko, K.; Neimark, A. V.; Olivier, J. P.; Rodriguez-Reinoso, F.; Rouquerol, J.; Sing, K. S. Physisorption of gases, with special reference to the evaluation of surface area and pore size distribution (IUPAC Technical Report). *Pure Appl. Chem.* **2015**, *87*, 1051–1069.

(30) (a) Peppas, N. Analysis of Fickian and non-Fickian drug release from polymers. *Pharm. Acta Helv.* **1983**, *60*, 110–111. (b) Korsmeyer, R. W.; Gurny, R.; Doelker, E.; Buri, P.; Peppas, N. A. Mechanisms of solute release from porous hydrophilic polymers. *Int. J. Pharm.* **1983**, *15*, 25–35.

(31) (a) Siepmann, J.; Peppas, N. A. Modeling of drug release from delivery systems based on hydroxypropyl methylcellulose (HPMC). *Adv. Drug Delivery Rev.* **1987**, *64*, 163–174. (b) Ritger, P. L.; Peppas, N. A. A simple equation for description of solute release II. Fickian and anomalous release from swellable devices. *J. Controlled Release* **1987**, *5*, 37–42.